JACS Au
AN OPEN ACCESS JOURNAL OF THE AMERICAN CHEMICAL SOCIETY

pubs.acs.org/jacsau
Article

DNA Framework-Engineered Assembly of Cyanine Dyes for Structural Identification of Nucleic Acids

Cong Li, Jielin Chen, Tiantian Man, Bin Chen, Jiang Li, Qian Li, Xiurong Yang, Ying Wan,* Chunhai Fan, and Jianlei Shen*

Cite This: *JACS Au* 2024, 4, 1125−1133
Read Online

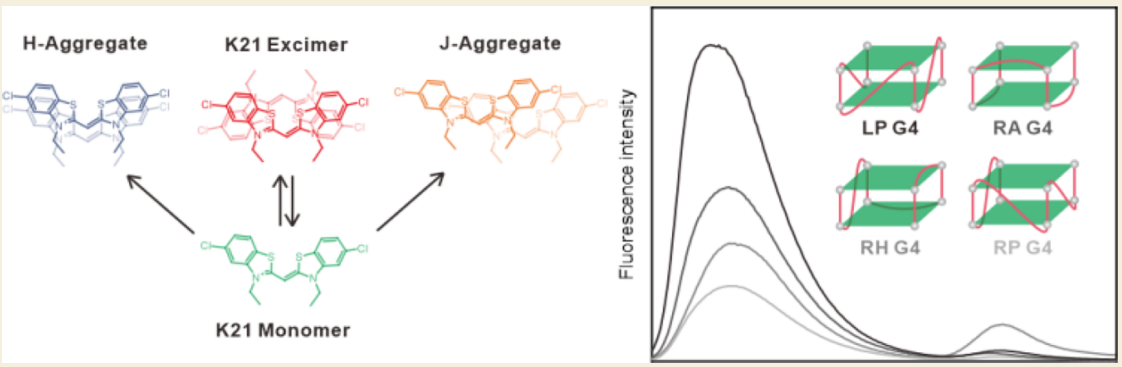

ABSTRACT: DNA nanostructures serve as precise templates for organizing organic dyes, enabling the creation of programmable artificial photonic systems with efficient light-harvesting and energy transfer capabilities. However, regulating the organization of organic dyes on DNA frameworks remains a great challenge. In this study, we investigated the factors influencing the self-assembly behavior of cyanine dye K21 on DNA frameworks. We observed that K21 exhibited diverse assembly modes, including monomers, H-aggregates, J-aggregates, and excimers, when combined with DNA frameworks. By manipulating conditions such as the ion concentration, dye concentration, and structure of DNA frameworks, we successfully achieved precise control over the assembly modes of K21. Leveraging K21's microenvironment-sensitive fluorescence properties on DNA nanostructures, we successfully discriminated between the chirality and topology structures of physiologically relevant G-quadruplexes. This study provides valuable insights into the factors influencing the dynamic assembly behavior of organic dyes on DNA framework nanostructures, offering new perspectives for constructing functional supramolecular aggregates and identifying DNA secondary structures.

KEYWORDS: *DNA frameworks, supramolecular aggregates, cyanine dyes, DNA secondary structures*

DNA nanostructure-based dye complexes offer exceptional functionality and hold immense potential across various fields, including light-harvesting,[1−4] energy transfer,[1,5−8] sensing,[9−15] imaging,[16−19] and cancer diagnosis.[20−23] Programmable DNA nanostructures provide a high degree of order and addressability, allowing precise control over the position, orientation, dynamics, and environment of dye molecules.[2,4,6,7,24] Consequently, DNA nanostructures serve as excellent templates for dye assembly, facilitating the creation of highly organized and densely packed supramolecular aggregates. For example, DNA nanostructures have been employed as chiral templates to impart chirality to dye aggregates.[25−27] More recently, a study reported that benzothiazole cyanine dye K21 and pseudoisocyanine (PIC) can form H-aggregates and J-aggregates on DNA templates, utilizing the exciton transfer properties of strongly coupled J-aggregates for long-range energy transfer.[1,28−31] However, the regulation of fluorescent dye organization on DNA frameworks remains challenging due to a limited understanding of the assembly factors involved.

Organic dye monomers typically bind to DNA through three primary modes: intercalation, groove binding, and external binding, facilitated by electrostatic and hydrophobic interactions.[32,33] Yan et al. have reported that K21 can noncovalently bind to the minor groove of DNA duplexes, forming J-aggregates.[30] J-aggregates are characterized by narrow, red-shifted absorption and emission bands and a shortened radiation lifetime compared to monomeric molecules. Conversely, H-aggregates exhibit a blue-shifted absorption band and reduced fluorescence emission intensity.[34] Furthermore, we have reported that K21 can also form an excimer state on DNA

Received: December 25, 2023
Revised: February 2, 2024
Accepted: February 7, 2024
Published: February 22, 2024

https://doi.org/10.1021/jacsau.3c00826
JACS Au 2024, 4, 1125−1133

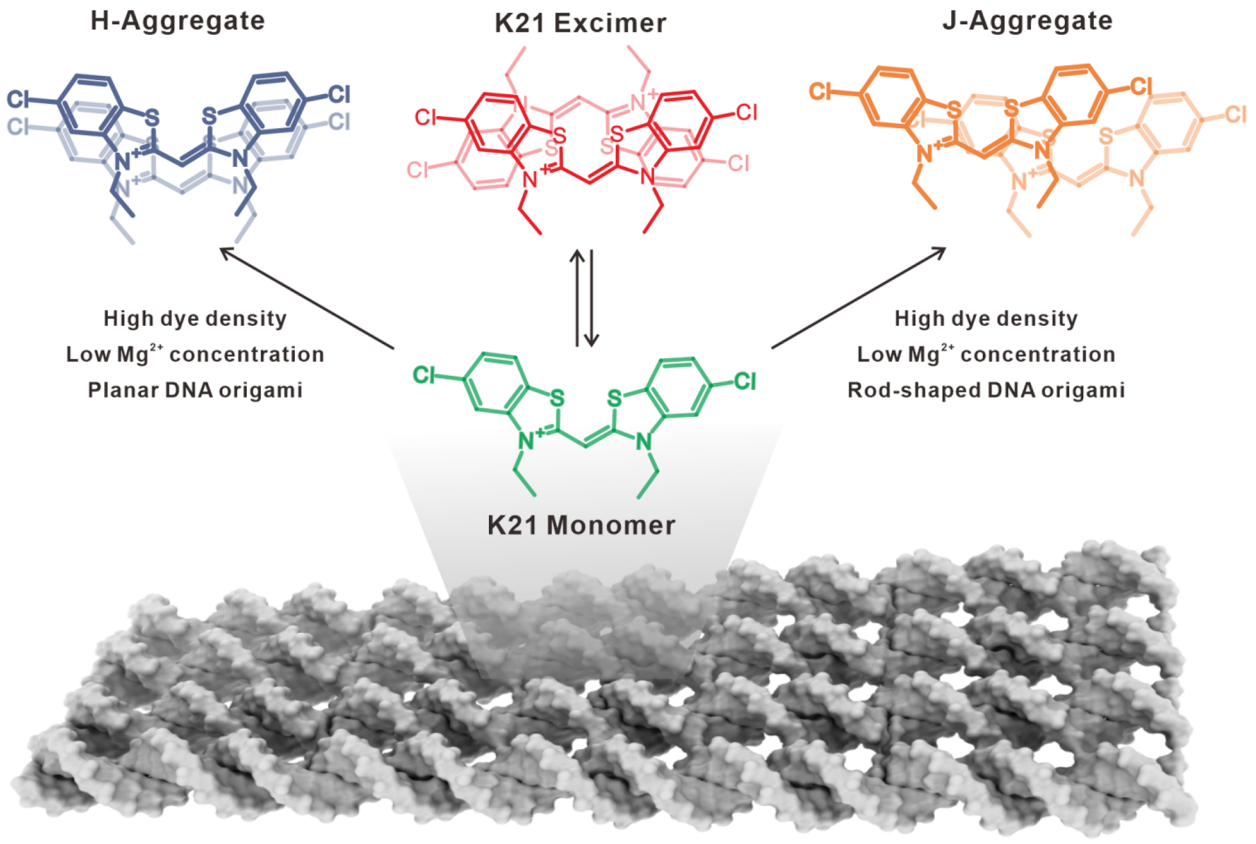

Figure 1. Schematic diagram of multiple assembly modes of K21 on the DNA framework. K21 can bind to DNA in the form of monomers, H-aggregates, J-aggregates, and excimers. Moreover, ion concentration, dye loading density, and DNA nanostructures can affect the assembly modes and fluorescence characteristics of K21. The chemical formulas for H/J-aggregate and excimer presented in our manuscript are hypothetical structures based on prior research.[34,35]

frameworks, and its fluorescence emission behavior is highly sensitive to transient conformational changes in DNA.[35] Excimers are transient species formed when two fluorophore molecules of the same type interact through π orbitals, with one in the excited state and the other in the ground state. Their formation is influenced by excitation and local concentration, resulting in red-shifted fluorescence characteristics compared to the monomer.[36] Despite our ability to control the assembly modes of organic dyes on DNA through factors like DNA sequence and dye concentration, there is still a need for systematic research on the diverse assembly modes of dyes on DNA and a deeper understanding of the factors influencing molecular assembly behavior.

In this study, we conducted a systematic investigation into the factors influencing the dynamic assembly of cyanine dye K21 on DNA frameworks. K21 displayed diverse assembly modes, including monomers, H-aggregates, J-aggregates, and excimers, when it self-assembled with DNA nanostructures (Figure 1). Through the manipulation of conditions such as magnesium ion concentration, dye loading density, and structure of DNA frameworks, we observed shifts in the assembly modes of K21, which affected the fluorescence emission intensity of both monomers and excimers. Furthermore, by harnessing the various assembly modes and fluorescence properties of K21 and DNA structures, we successfully discerned the chirality of G-quadruplex (G4) topology and identified subtle structural differences among G4s of the same folding type. Hence, our work provides novel insights into the dynamic assembly behavior of organic dyes on DNA frameworks, thereby aiding in the design of biomimetic photonic systems and the identification of multiple secondary structures within nucleic acids.

CONSTRUCTION AND CHARACTERIZATION OF MULTIPLE ASSEMBLY MODES OF K21 ON THE DNA FRAMEWORK

To investigate the multiassembly modes of K21 on DNA, we synthesized 10H (helix) × 10H (helix) DNA brick crystals as assembly templates for K21.[37] The one-dimensional DNA brick crystals were assembled from 32-nucleotide (nt) single-stranded DNA bricks, featuring 10H × 10H square-shaped cross sections. The selection of 10H × 10H DNA brick crystals as templates for K21 assembly stems from their microscale length, enabling the direct observation of dye distribution on DNA nanostructures under fluorescence imaging microscopy. A one-pot annealing process was carried out in the presence of 40 mM $MgCl_2$ for 72 h, resulting in the self-assembly of unpurified DNA strands into 10H × 10H structures (Figure 2a). These structures were then purified through ultrafiltration and transferred to a buffer with a lower magnesium ion concentration. After incubating DNA nanostructures with K21 at a final concentration of 37 μM (a molar ratio of 4:1, DNA base pairs to K21), transmission electron microscopy (TEM) images of the unpurified mixtures show highly uniform 10H × 10H DNA brick structures, with no discernible large aggregate particles or disordered assembly (Figure 2b and Figure S1).

Next, we investigated the photophysical properties of K21 when it was incubated with DNA bricks. In contrast to the

https://doi.org/10.1021/jacsau.3c00826
JACS Au 2024, 4, 1125−1133

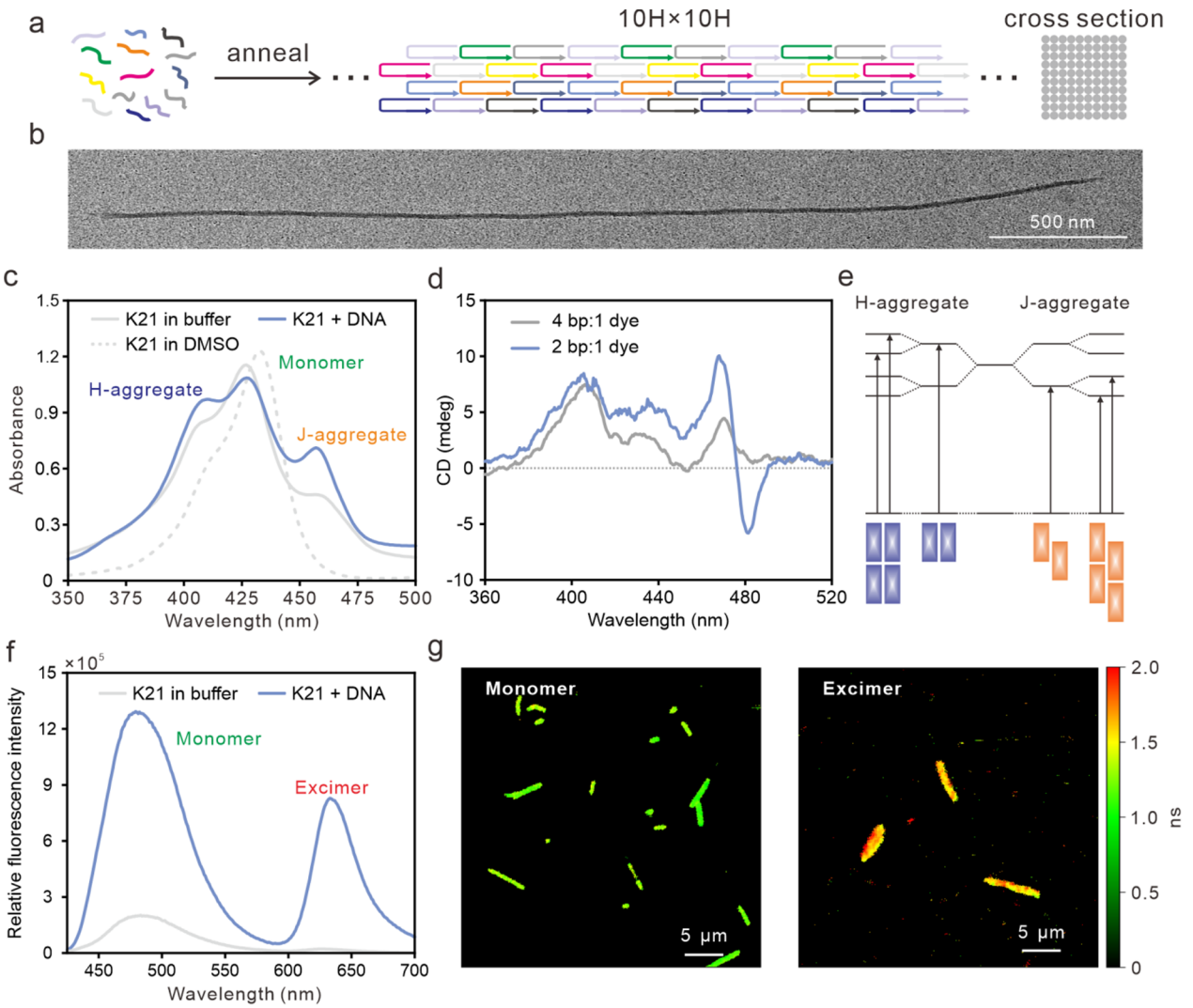

Figure 2. Formation and characterization of multiple assembly modes of K21 on DNA frameworks. (a) Schematic depiction of the assembly of 10H × 10H brick crystals. (b) TEM image of DNA brick crystals binding to K21. Scale bar: 500 nm. (c) Absorption spectra comparing free K21 in DMSO (37 μM), K21 (37 μM) in aqueous DNA nanostructure buffer (5 mM Tris, 1 mM EDTA, and 12.5 mM $MgCl_2$, pH 8.0), and K21 (37 μM) after incubation of DNA brick crystals. (d) CD spectra of DNA brick crystals incubated with varying concentrations of K21 (37 and 74 μM). (e) Exciton-coupling models explaining the relationship between spectral shifts and aggregation structures. (f) Emission spectra showing a comparison between free K21 (37 μM) and K21 incubated with DNA brick crystals (4 bp: 1 dye). The reaction buffer includes 5 mM Tris, 1 mM EDTA, and 12.5 mM $MgCl_2$, pH 8.0. λ_{ex} = 411 nm. (g) FLIM images of K21 monomer and excimer on DNA brick crystals. The 480−520 nm emission filter was used for detection of monomer, and a 595−635 nm emission filter was used for detection of excimer. λ_{ex} = 405 nm.

absorption spectra of free K21, which exhibits a maximum absorption at 427 nm, the absorption peak of the DNA-bound K21 monomer decreases. Simultaneously, there is an increase in absorption peaks at 409 and 457 nm (Figure 2c,e). These blue/red-shifted absorption bands at 409 and 457 nm are attributed to the formation of H-aggregates and J-aggregates, as reported previously.[38] In a recent study, Lan et al. substantiated the formation of K21 H/J-aggregates on a DNA template by employing all-atom molecular dynamics (MD) simulation. They observed the appearance of blue/red-shifted absorption bands at 408 and 472 nm, respectively.[39] To further validate the presence of aggregates on DNA scaffolds, we conducted circular dichroism (CD) spectral measurements of the K21-DNA complex at various ratios (Figure 2d). At low dye density, a positive CD signal from 360 to 520 nm was observed, which indicated that the ligand was bound in the minor groove of B-DNA, with a transition moment oriented along the groove,[40] similar to that of DNA minor-groove binders, Hoechst,[41] and DAPI.[42] As the dye concentration increased, K21 exhibited a bisignate Cotton effect at longer wavelengths, indicative of exciton-coupled CD arising from exciton−exciton coupling—a characteristic feature of J-aggregate formation[39] (Figure 2d,e). A similar phenomenon was previously observed in studies on the formation of J-aggregates on DNA using the PIC dye.[43,44] However, PIC dye tends to form aggregates in poly(dA)−poly(dT) dinucleotide tracks whereas K21 exhibits negligible sequence selectivity.[29,30] Moreover, the negative signal from H-aggregates may have been concealed by the positive signal from the monomers (Figure 2d).

Furthermore, upon binding to DNA, the fluorescence emission intensities of the K21 monomer and excimer increased by 6.9 and 42.2 times, respectively (as shown in Figure 2f). This indicates a robust noncovalent interaction between the K21 monomer and DNA. The constrained environment provided by

https://doi.org/10.1021/jacsau.3c00826
JACS Au 2024, 4, 1125−1133

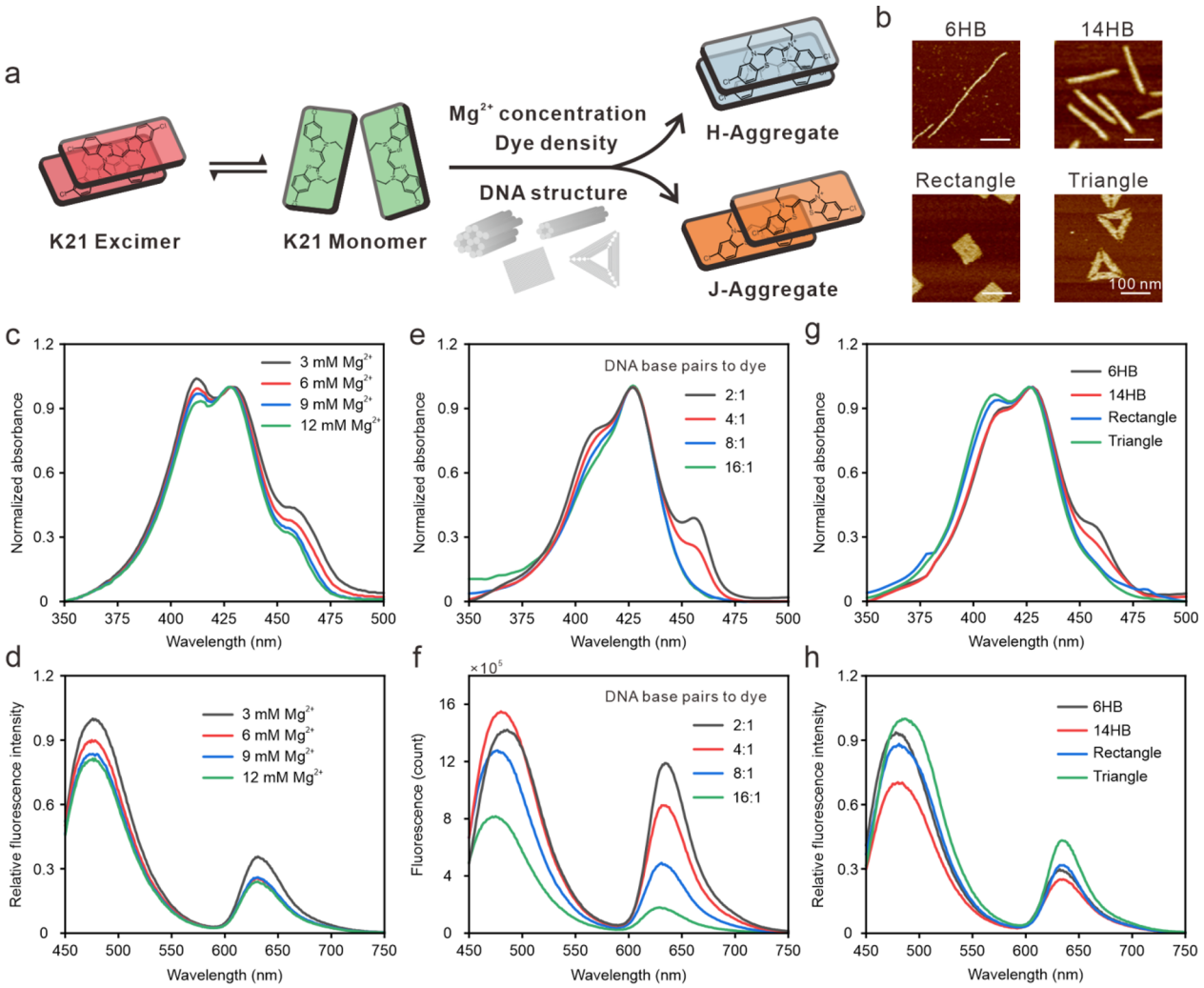

Figure 3. Regulation of assembly modes and fluorescence characteristics of K21-DNA origami under different conditions. (a) Schematic diagram of the effects of ion strength, dye density, and DNA structure on the assembly modes and fluorescence characteristics of K21. (b) AFM images of four DNA origami nanostructures (6HB, 14HB, rectangle, triangle). Scale bar: 100 nm. (c, d) Absorption spectra and relative fluorescence emission spectra of the K21−6HB complex at different Mg^{2+} concentrations. (e, f) Absorption spectra and emission spectra of 6HB incubated with varying K21 concentrations. (g, h) Absorption spectra and relative fluorescence emission spectra of different DNA origami nanostructures when incubated with K21. The fluorescence emission intensities of each sample in (d) and (h) were scaled by dividing the intensity by the absorptance (i.e., 1 − transmittance) at the excitation wavelength. The concentrations of DNA origami and K21 in experiments were 10 nM and 18.5 μM for (c), (d), (g), and (h), respectively. The concentrations of K21 used in (e) and (f) were 2.3, 4.6, 9.2, and 18.5 μM, corresponding to DNA base pair to dye ratios of 16:1, 8:1, 4:1, and 2:1, respectively. The excitation wavelength was 411 nm.

DNA induces K21 to adopt a more rigid and planar conformation upon insertion into the DNA groove, thereby restricted the intramolecular motion or rotation of K21.[45] Moreover, the elevated local concentration of K21 in DNA promotes the formation of K21 excimers. The results align well with prior study,[35] indicating K21's robust binding affinity for double-stranded DNA. This binding capability may impede the self-aggregation of K21 in the solution. Fluorescence lifetime imaging microscopy (FLIM) is a powerful technique employed to discern the distinctive fluorophores. This method gauges the duration for which a fluorophore stays in an excited state before emitting a photon, providing valuable insights into molecular characteristics. FLIM imaging results reveal the localization of photoluminescence from the 480−520 nm emission channel and the 595−635 nm emission channel (λ_{ex} = 405 nm) on DNA nanostructures, with fluorescence lifetimes of approximately 1.0 ± 0.06 and 1.5 ± 0.09 ns, respectively (Figures 2g and Figure S3). The FLIM results highlight the localization of two emissive species on DNA nanostructures, and the lifetimes of these two species are consistent with monomer and excimers reported in a previous study[35] (Figures 2g and Figure S2). It is essential to note that, owing to the pronounced photobleaching effect of K21 during FLIM measurements, it became imperative to reposition and conduct separate fluorescence imaging of monomers and excimers on the DNA nanostructure. In summary, these experimental findings confirm that K21 can engage with DNA in multiple assembly modes, including monomers, H-aggregates, J-aggregates, and excimers.

REGULATION OF ASSEMBLY MODES AND FLUORESCENCE CHARACTERISTICS OF THE K21−DNA COMPLEX

Next, we aimed to control the assembly modes and fluorescence properties of K21 in conjunction with the DNA nanostructures. We systematically examined the influence of magnesium ion

https://doi.org/10.1021/jacsau.3c00826
JACS Au 2024, 4, 1125−1133

concentration, dye loading density, and DNA nanostructures on the absorption and emission characteristics of K21 (Figure 3a). Due to the lack of controllability over the length of DNA brick crystals, we opted for the use of the structurally well-defined 6HB DNA origami as the template for regulating the assembly modes of K21. The 6HB DNA origami is a 400 nm-long DNA structure, comprising a six-helix bundle arranged in a honeycomb lattice. It was created through the folding of long, single-stranded DNA (M13mp18 scaffold, 7249 nt) with the assistance of a custom set of short single-stranded DNA (ssDNA). Initially, as the magnesium ion concentration gradually increased, the absorption intensity of both H-aggregates and J-aggregates of K21 on six-helix bundle (6HB) DNA origami decreased, which was normalized relative to the absorption peak of the monomer (Figure 3c). Furthermore, the fluorescence emission intensity of both the monomer and excimer also decreased gradually (Figure 3d). These observations indicated that magnesium ions could attenuate the electrostatic interaction between the negatively charged DNA phosphate backbone and positively charged K21 molecules, thereby impeding the binding of K21 to DNA.

Furthermore, with the increasing loading density of K21 molecules on 6HB DNA origami, we initially observed a rise in absorption intensity at 409 nm (Figure 3e). Further elevation of the K21 concentration results in a simultaneous increase in absorption intensity at both 409 and 457 nm (Figure 3e). The initial appearance of absorption at 409 nm indicates the presence of H-aggregates before the formation of both H-aggregates and J-aggregates. In contrast, similar concentration increases of K21 in the organic solvent, dimethyl sulfoxide (DMSO), do not produce any noticeable change in the shape of the absorption spectra (Figure S4), suggesting the excellent solubility of K21 in DMSO. Furthermore, the augmentation in the absorption intensity of both H-aggregates and J-aggregates in the reaction buffer is much weaker when juxtaposed with the same concentration of K21 in the solution of DNA nanostructures (Figure S5). These observations suggest that the DNA template could promote the formation of H-/J-aggregates, a notion further supported by the absorption and CD spectra presented in Figure 2c,d. Simultaneously, with the increase in K21 concentration, the fluorescence emission intensity of the monomer initially rises, reaching its peak when the molar ratio of DNA base pairs to K21 molecules stands at 4:1. However, further increments in K21 concentration diminish the emission intensity of the monomer (Figure 3f), possibly due to fluorescence quenching between dye molecules at higher dye concentrations. Similar fluorescence quenching phenomena of K21 were observed in previous reports at higher dye concentrations.[46] Notably, as the K21 concentration increases, the normalized fluorescence emission peak of the monomer gradually shifts toward the red end of the spectra, indicating the progressive formation of J-aggregates[34] (Figure S6). As a control, we observed that the increase in the K21 concentration in the reaction buffer resulted in a linear increase in fluorescence intensity and induced a slight shift of the emission peak to longer wavelengths (Figure S7). This observation effectively rules out inner filter effects on the experimental outcomes and suggests a weak influence of changes in the solvent environment. However, in contrast to the monomer, the fluorescence emission intensity of the excimer steadily increases with a rising K21 concentration (Figure 3f). This illustrates that a high concentration of dye on 6HB DNA origami enhances intermolecular interactions, facilitating the formation of the excimer without encountering intermolecular fluorescence quenching.

We then investigated the assembly modes and fluorescence properties of K21 on four types of DNA origami: two rod-shaped structures (6HB, 14HB, one-dimensional) and two planar structures (rectangle, triangle, two-dimensional) (Figure 3b). AFM images show that the morphology of the DNA origami remained intact after binding with K21 (Figure S8) and the height of the rectangle DNA origami increased by ∼0.9 nm (Figure S9). In the normalized absorption spectra, the one-dimensional rod-shaped DNA origami structures (6HB and 14HB) exhibited stronger absorption at 457 nm while the weak absorption at 409 nm, indicating a preference for promoting the formation of J-aggregates. In contrast, the two-dimensional planar DNA origami structures (rectangle and triangle) exhibits negligible absorption at 457 nm and greatly enhanced absorption at 409 nm, suggesting that the two-dimensional planar DNA origami facilitated the formation of H-aggregates by K21 (Figure 3g). This preference for a particular organizational mode on different DNA nanostructures was attributed to the distinctive arrangement of the DNA origami bundles. The double-helix bundles of one-dimensional rod-shaped DNA origami extend to both ends in a spiral manner, providing a favorable environment for K21 to form head-to-tail J-aggregate structures. The double-helix bundles of two-dimensional planar DNA origami are arranged and extended side by side, promoting the formation of face-to-face H-aggregate structures[47] (as shown in Figure 2e). Considering the relatively larger size of DNA duplexes compared to K21, the spatial alignment of duplexes within a DNA superstructure may influence the aggregation forms of dye molecules by modulating the transient conformations of local DNA duplexes on DNA nanostructures.[35] Moreover, under the same concentration of DNA origami and K21, in comparison to the one-dimensional rod-shaped DNA origami, the combination of K21 with two-dimensional planar DNA origami resulted in a higher fluorescence emission intensity and quantum yield (QY) for both the monomer and excimer (Figure 3h and Table S1). This difference may be attributed to the specific surface area of the DNA origami structures. For instance, 14HB, with its larger diameter and denser, more rigid structure, had a relatively smaller binding area with K21, leading to weaker fluorescence intensity for both the monomer and excimer compared to 6HB. To further substantiate our speculation, we designed and synthesized two new DNA origamis: a two-dimensional Cross DNA origami and a one-dimensional 24HB DNA origami (Figure S10). When K21 interacts with these two types of DNA origami, Cross DNA origami proves to be more conducive to inducing the formation of H-aggregates while 24HB promotes the formation of J-aggregates. Additionally, due to its smaller structural specific surface area, 24HB exhibits weaker monomer and excimer fluorescence intensity (Figure S11).

DISCRIMINATION AND CLASSIFICATION OF STRUCTURALLY SIMILAR G-QUADRUPLEXES

Beyond the conventional double helix, nucleic acids have the capacity to form intricate secondary structures, among which G-quadruplexes (G4s) are notable. G4s are noncanonical secondary structures constituted by four strands within guanine-rich nucleic acid sequences.[48,49] Their significance extends to the regulation of biological structure and function, encompassing genetic translation, telomere preservation, and genomic stability.[50,51] Intriguingly, G4s can adopt both right-handed and left-handed helical configurations.[52] Previous studies have employed small-molecule ligands to identify G4s

https://doi.org/10.1021/jacsau.3c00826
JACS Au 2024, 4, 1125−1133

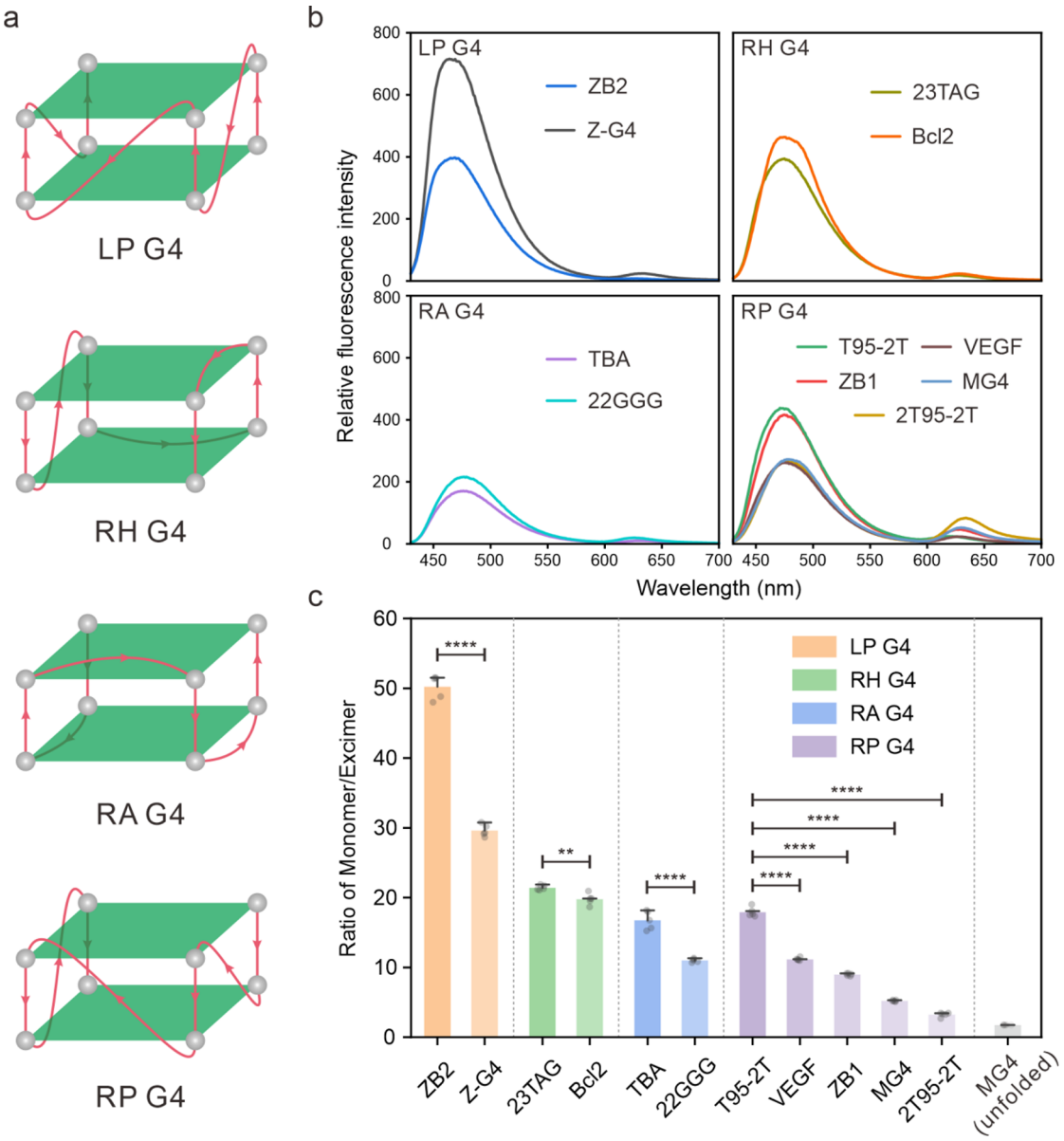

Figure 4. Ratiometric fluorescence-based discrimination of variable DNA G4 structures. (a) Schematic representations of four distinct G4 structures (LP G4: left-handed parallel G-quadruplex; RH G4: right-handed hybrid G-quadruplex; RA G4: right-handed antiparallel G-quadruplex; RP G4: right-handed parallel G-quadruplex). (b) Fluorescence spectra of different G4 structures combined with K21 (each curve is averaged by five sets of parallel samples). The concentrations of DNA G4 bases and K21 were 140 and 35 μM, respectively. Excitation was at 411 nm. (c) The graph illustrates the ratio of emission intensity between the monomer and excimer following the incubation of K21 with various G4 structures. $n = 5$. Data represent mean ± standard deviation. $^{**}P < 0.01$; $^{****}P < 0.0001$. The reaction buffer used for the formation of different G4 structures containing 70 mM KCl, 20 mM potassium phosphate buffer (pH 7.0).

by leveraging $\pi-\pi$ stacking interactions with G tetrads and binding to grooves or rings.[53,54] However, these approaches encounter challenges when it comes to directly distinguishing between various secondary structures of G4s and discerning their chirality. Therefore, in this study, we harnessed environmentally sensitive self-organization behavior to discriminate even minor structural differences in G4s. This enabled us to successfully identify and detect the chirality and topology of G4s by using fluorescence readouts as a diagnostic tool.

We classify the G4 structures into four types based on the direction of the chain and the isomerization of the glycosidic bond: left-handed parallel (ZB2, Z-G4), right-handed hybrid (23TAG, Bcl2), right-handed antiparallel (TBA, 22GGG), and right-handed parallel (T95-2T, VEGF, ZB1, MG4, and 2T95-2T) (Figure 4a). We optimized the molar ratio of K21 combined with G4s and found that the maximum fluorescence emission intensity of the K21 monomer was achieved at a molar ratio of 4:1 (the number of G4s bases to K21 molecules) (Figure S12). Subsequently, we obtained normalized absorption and emission spectra of K21 incubated with different G4 structures (Figure S14). Among them, the fluorescence intensity ratio of monomer to excimer revealed that K21 exhibited a higher binding affinity toward the left-handed parallel G4s structures compared to other topologies (Figure 4b,c). Previous studies have shown that small organic molecules preferentially bind to the parallel G4 structures, resulting in a stronger fluorescence response.[53] Moreover, excimer was highly sensitive to the transient conformational stability of DNA structures. Interestingly, K21

https://doi.org/10.1021/jacsau.3c00826
JACS Au 2024, 4, 1125−1133

demonstrated the ability to respond to the chirality of the G4 structures compared to other dye molecules, as indicated by the lower fluorescence ratio for right-handed parallel G4s (Figure 4c). These suggest that K21 can specifically recognize the direction of the G4 oligonucleotide chain's rotation. Furthermore, our strategy effectively distinguishes different G4 structures within the same folding type, demonstrating our successful distinction of the structural chirality of G4s and the identification of small structural differences within G4s of the same folding type (Figure 4b,c). To further substantiate this hypothesis, we employed K21 to discriminate between different chiral structures of G4s with identical sequences. The 22AG G4 structure, derived from the human telomeric sequence featuring repetitive nucleotide sequences of T2AG3 at each end of the chromosome, exhibits distinct conformations. In the presence of K^+, the structure adopts a right-handed hybrid topology, while in the presence of Na^+, it assumes a right-handed antiparallel topology.[55] Following incubation of K21 with both structures, K21 demonstrated a higher fluorescence intensity ratio of monomer to excimer in the solution of the right-handed hybrid G4 structures compared to the right-handed antiparallel G4s (Figure S15).

To eliminate potential interference from free K21 in the solution and assess the system's robustness against contaminants, we examined the fluorescence changes of K21 in the presence of both folded G4 and unfolded G4 structures. Additionally, we monitored fluorescence changes after the introduction of various concentrations of ssDNA contaminants. The fluorescence spectra (Figure S13) demonstrated that K21 exhibited a substantial fluorescence enhancement with folded G4 structures compared to the unfolded ssDNA form. Importantly, the recognition of G4 structures by K21 remained unaffected by the presence of various concentrations of nucleotide contaminants such as ssDNA (Figure S16).

In conclusion, we systematically explored the factors influencing the dynamic organization of the organic dye K21 on DNA, enabling the precise identification of the chiral topology of G4s. The DNA framework served as a template for the self-assembly of K21, resulting in diverse assembly modes, including monomers, H-aggregates, J-aggregates, and excimers, each exhibiting distinctive fluorescence properties. By manipulating variables such as the ionic strength, dye loading density, and structure of DNA frameworks, we induced significant variations in the interactions between K21 and DNA, thereby causing noticeable alterations in the fluorescence emission intensity of K21 monomers and excimers. This microenvironment-sensitive organizational system was effectively employed to discriminate the chirality of G4s' topology and detect subtle structural differences within G4s of the same folding type. Our study not only provides fresh insights into the regulation of organizational modes of functional dyes on DNA frameworks but also holds promise for applications in biomimetic photonic systems, nucleic acid secondary structure identification, and single-molecule analysis.

■ ASSOCIATED CONTENT

Supporting Information

The Supporting Information is available free of charge at https://pubs.acs.org/doi/10.1021/jacsau.3c00826.

Experimental section; additional figures; and table (PDF)

■ AUTHOR INFORMATION

Corresponding Authors

Ying Wan − *School of Mechanical Engineering, Nanjing University of Science and Technology, Nanjing 210094, China;* orcid.org/0000-0002-3409-0492; Email: wanying@njust.edu.cn

Jianlei Shen − *School of Chemistry and Chemical Engineering, New Cornerstone Science Laboratory, Frontiers Science Center for Transformative Molecules and National Center for Translational Medicine, Shanghai Jiao Tong University, Shanghai 200240, China;* orcid.org/0000-0001-6386-5640; Email: shenjianlei@sjtu.edu.cn

Authors

Cong Li − *School of Chemistry and Chemical Engineering, New Cornerstone Science Laboratory, Frontiers Science Center for Transformative Molecules and National Center for Translational Medicine, Shanghai Jiao Tong University, Shanghai 200240, China*

Jielin Chen − *School of Chemistry and Chemical Engineering, New Cornerstone Science Laboratory, Frontiers Science Center for Transformative Molecules and National Center for Translational Medicine, Shanghai Jiao Tong University, Shanghai 200240, China*

Tiantian Man − *School of Mechanical Engineering, Nanjing University of Science and Technology, Nanjing 210094, China*

Bin Chen − *School of Material Science and Chemical Engineering, Ningbo University, Ningbo, Zhejiang 315211, China*

Jiang Li − *Institute of Materiobiology, Department of Chemistry, College of Science, Shanghai University, Shanghai 200444, China*

Qian Li − *School of Chemistry and Chemical Engineering, New Cornerstone Science Laboratory, Frontiers Science Center for Transformative Molecules and National Center for Translational Medicine, Shanghai Jiao Tong University, Shanghai 200240, China*

Xiurong Yang − *School of Chemistry and Chemical Engineering, New Cornerstone Science Laboratory, Frontiers Science Center for Transformative Molecules and National Center for Translational Medicine, Shanghai Jiao Tong University, Shanghai 200240, China; State Key Laboratory of Electroanalytical Chemistry, Changchun Institute of Applied Chemistry, Chinese Academy of Sciences, Changchun, Jilin 130022, China;* orcid.org/0000-0003-0021-5135

Chunhai Fan − *School of Chemistry and Chemical Engineering, New Cornerstone Science Laboratory, Frontiers Science Center for Transformative Molecules and National Center for Translational Medicine, Shanghai Jiao Tong University, Shanghai 200240, China;* orcid.org/0000-0002-7171-7338

Complete contact information is available at: https://pubs.acs.org/10.1021/jacsau.3c00826

Author Contributions

The manuscript was written through the contributions of all authors. All authors have given approval to the final version of the manuscript. CRediT: **Cong Li** investigation, methodology, writing-original draft; **Jielin Chen** data curation, methodology, visualization; **Tiantian Man** investigation, validation; **Bin Chen** data curation, writing-review & editing; **Jiang Li** conceptualization, resources; **Qian Li** resources, writing-review & editing;

https://doi.org/10.1021/jacsau.3c00826
JACS Au 2024, 4, 1125−1133

Xiurong Yang project administration, resources; **ying wan** conceptualization, supervision, writing-review & editing; **Chunhai Fan** project administration, resources; **Jianlei Shen** conceptualization, funding acquisition, project administration, supervision, writing-review & editing.

Notes

The authors declare no competing financial interest.

■ ACKNOWLEDGMENTS

This work was financially supported by the National Key R&D Program of China (2020YFA0908104, 2018YFA0902600), the National Natural Science Foundation of China (21834007, 21904087, T2188102), and the Shanghai Municipal Science and Technology Commission (21QA1404800, 20dz1101000).

■ REFERENCES

(1) Zhou, X.; Satyabola, D.; Liu, H.; Jiang, S. X.; Qi, X. D.; Yu, L.; Lin, S.; Liu, Y.; Woodbury, N. W.; Yan, H. Two-Dimensional Excitonic Networks Directed by DNA Templates as an Efficient Model Light-Harvesting and Energy Transfer System. *Angew. Chem., Int. Ed.* **2022**, *61*, e202211200.

(2) Dutta, P. K.; Varghese, R.; Nangreave, J.; Lin, S.; Yan, H.; Liu, Y. DNA-Directed Artificial Light-Harvesting Antenna. *J. Am. Chem. Soc.* **2011**, *133*, 11985−11993.

(3) Woller, J. G.; Hannestad, J. K.; Albinsson, B. Self-Assembled Nanoscale DNA-Porphyrin Complex for Artificial Light Harvesting. *J. Am. Chem. Soc.* **2013**, *135*, 2759−2768.

(4) Buckhout-White, S.; Spillmann, C. M.; Algar, W. R.; Khachatrian, A.; Melinger, J. S.; Goldman, E. R.; Ancona, M. G.; Medintz, I. L. Assembling Programmable FRET-based photonic Networks using Designer DNA Scaffolds. *Nat. Commun.* **2014**, *5*, 5615.

(5) Hannestad, J. K.; Sandin, P.; Albinsson, B. Self-Assembled DNA photonic Wire for Long-Range Energy Transfer. *J. Am. Chem. Soc.* **2008**, *130*, 15889−15895.

(6) Stein, I. H.; Steinhauer, C.; Tinnefeld, P. Single-Molecule Four-Color FRET Visualizes Energy-Transfer Paths on DNA Origami. *J. Am. Chem. Soc.* **2011**, *133*, 4193−4195.

(7) Nicoli, F.; Barth, A.; Bae, W.; Neukirchinger, F.; Crevenna, A. H.; Lamb, D. C.; Liedl, T. Directional photonic Wire Mediated by Homo-Forster Resonance Energy Transfer on a DNA Origami Platform. *ACS Nano* **2017**, *11*, 11264−11272.

(8) Hart, S. M.; Chen, W. J.; Banal, J. L.; Bricker, W. P.; Dodin, A.; Markova, L.; Vyborna, Y.; Willard, A. P.; Häner, R.; Bathe, M.; Schlau-Cohen, G. S. Engineering Couplings for Exciton Transport using Synthetic DNA Scaffolds. *Chem.* **2021**, *7*, 752−773.

(9) Trofymchuk, K.; Glembockyte, V.; Grabenhorst, L.; Steiner, F.; Vietz, C.; Close, C.; Pfeiffer, M.; Richter, L.; Schütte, M. L.; Selbach, F.; Yaadav, R.; Zähringer, J.; Wei, Q.; Ozcan, A.; Lalkens, B.; Acuna, G. P.; Tinnefeld, P. Addressable Nanoantennas with Cleared Hotspots for Single-Molecule Detection on a Portable Smartphone Microscope. *Nat. Commun.* **2021**, *12*, 950.

(10) Ochmann, S. E.; Joshi, H.; Buber, E.; Franquelim, H. G.; Stegemann, P.; Sacca, B.; Keyser, U. F.; Aksimentiev, A.; Tinnefeld, P. DNA Origami Voltage Sensors for Transmembrane Potentials with Single-Molecule Sensitivity. *Nano Lett.* **2021**, *21*, 8634−8641.

(11) Huang, Q. L.; Chen, B.; Shen, J. L.; Liu, L.; Li, J. J.; Shi, J. Y.; Li, Q.; Zuo, X. L.; Wang, L. H.; Fan, C. H.; Li, J. Encoding Fluorescence Anisotropic Barcodes with DNA Fameworks. *J. Am. Chem. Soc.* **2021**, *143*, 10735−10742.

(12) Liu, J.; Cao, Z.; Lu, Y. Functional Nucleic Acid Sensors. *Chem. Rev.* **2009**, *109*, 1948−1998.

(13) Idili, A.; Vallée-Bélisle, A.; Ricci, F. Programmable pH-Triggered DNA Nanoswitches. *J. Am. Chem. Soc.* **2014**, *136*, 5836−5839.

(14) Cao, Y. C.; Jin, R.; Nam, J.-M.; Thaxton, C. S.; Mirkin, C. A. Raman Dye-Labeled Nanoparticle Probes for Proteins. *J. Am. Chem. Soc.* **2003**, *125*, 14676−14677.

(15) Xia, F.; Zuo, X.; Yang, R.; Xiao, Y.; Kang, D.; Vallée-Bélisle, A.; Gong, X.; Heeger, A. J.; Plaxco, K. W. On the Binding of Cationic, Water-Soluble Conjugated Polymers to DNA: Electrostatic and Hydrophobic Interactions. *J. Am. Chem. Soc.* **2010**, *132*, 1252−1254.

(16) Liu, J.; Jing, X.; Liu, M.; Li, F.; Li, M.; Li, Q.; Shi, J.; Li, J.; Wang, L.; Mao, X.; Zuo, X.; Fan, C. Mechano-Fluorescence Actuation in Single Synaptic Vesicles with a DNA Framework Nanomachine. *Sci. Robot.* **2022**, *7*, eabq5151.

(17) Lin, C. X.; Jungmann, R.; Leifer, A. M.; Li, C.; Levner, D.; Church, G. M.; Shih, W. M.; Yin, P. Submicrometre Geometrically Encoded Fluorescent Barcodes Self-assembled from DNA. *Nat. Chem.* **2012**, *4*, 832−839.

(18) Kishi, J. Y.; Lapan, S. W.; Beliveau, B. J.; West, E. R.; Zhu, A.; Sasaki, H. M.; Saka, S. K.; Wang, Y.; Cepko, C. L.; Yin, P. SABER Amplifies FISH: Enhanced Multiplexed Imaging of RNA and DNA in Cells and Tissues. *Nat. Methods* **2019**, *16*, 533−544.

(19) Liu, Z.; Pei, H.; Zhang, L.; Tian, Y. Mitochondria-Targeted DNA Nanoprobe for Real-Time Imaging and Simultaneous Quantification of Ca2+ and pH in Neurons. *ACS Nano* **2018**, *12*, 12357−12368.

(20) Zhuang, X.; Ma, X.; Xue, X.; Jiang, Q.; Song, L.; Dai, L.; Zhang, C.; Jin, S.; Yang, K.; Ding, B.; Wang, P.; Liang, X. A Photosensitizer-Loaded DNA Origami Nanosystem for Photodynamic Therapy. *ACS Nano* **2016**, *10*, 3486−3495.

(21) Song, L.; Jiang, Q.; Liu, J.; Li, N.; Liu, Q.; Dai, L.; Gao, Y.; Liu, W.; Liu, D.; Ding, B. DNA Origami/Gold Nanorod Hybrid nanostructures for the Circumvention of Drug Resistance. *Nanoscale* **2017**, *9*, 7750−7754.

(22) Jiang, Q.; Liu, S.; Liu, J.; Wang, Z. G.; Ding, B. Rationally Designed DNA-Origami Nanomaterials for Drug Delivery In Vivo. *Adv. Mater.* **2019**, *31*, 1804785.

(23) Shen, L.; Wang, P.; Ke, Y. DNA Nanotechnology-Based Biosensors and Therapeutics. *Adv. Healthcare Mater.* **2021**, *10*, 2002205.

(24) Zhan, P. F.; Peil, A.; Jiang, Q.; Wang, D. F.; Mousavi, S.; Xiong, Q. C.; Shen, Q.; Shang, Y. X.; Ding, B. Q.; Lin, C. X.; Ke, Y. G.; Liu, N. Recent Advances in DNA Origami-Engineered Nanomaterials and Applications. *Chem. Rev.* **2023**, *123*, 3976−4050.

(25) Jiang, Q.; Xu, X. H.; Yin, P. A.; Ma, K.; Zhen, Y. G.; Duan, P. F.; Peng, Q.; Chen, W. Q.; Ding, B. Q. Circularly Polarized Luminescence of Achiral Cyanine Molecules Assembled on DNA Templates. *J. Am. Chem. Soc.* **2019**, *141*, 9490−9494.

(26) Duncan, K. M.; Byers, H. M.; Houdek, M. E.; Roy, S. K.; Biaggne, A.; Barclay, M. S.; Patten, L. K.; Huff, J. S.; Kellis, D. L.; Wilson, C. K.; Lee, J.; Davis, P. H.; Mass, O. A.; Li, L.; Turner, D. B.; Hall, J. A.; Knowlton, W. B.; Yurke, B.; Pensack, R. D. Electronic Structure and Excited-State Dynamics of DNA-Templated Monomers and Aggregates of Asymmetric Polymethine Dyes. *J. Phys. Chem. A* **2023**, *127*, 4901−4918.

(27) Chowdhury, A. U.; Díaz, S. A.; Huff, J. S.; Barclay, M. S.; Chiriboga, M.; Ellis, G. A.; Mathur, D.; Patten, L. K.; Sup, A.; Hallstrom, N.; Cunningham, P. D.; Lee, J.; Davis, P. H.; Turner, D. B.; Yurke, B.; Knowlton, W. B.; Medintz, I. L.; Melinger, J. S.; Pensack, R. D. Tuning between Quenching and Energy Transfer in DNA-Templated Heterodimer Aggregates. *J. Phys. Chem. Lett.* **2022**, *13*, 2782−2791.

(28) Banal, J. L.; Kondo, T.; Veneziano, R.; Bathe, M.; Schlau-Cohen, G. S. Photophysics of J-Aggregate-Mediated Energy Transfer on DNA. *J. Phys. Chem. Lett.* **2017**, *8*, 5827−5833.

(29) Boulais, E.; Sawaya, N. P. D.; Veneziano, R.; Andreoni, A.; Banal, J. L.; Kondo, T.; Mandal, S.; Lin, S.; Schlau-Cohen, G. S.; Woodbury, N. W.; Yan, H.; Aspuru-Guzik, A.; Bathe, M. Programmed Coherent Coupling in a Synthetic DNA-based Excitonic Circuit. *Nat. Mater.* **2018**, *17*, 159−166.

(30) Zhou, X.; Mandal, S.; Jiang, S. X.; Lin, S.; Yang, J. Z.; Liu, Y.; Whitten, D. G.; Woodbury, N. W.; Yan, H. Efficient Long-Range, Directional Energy Transfer through DNA-Templated Dye Aggregates. *J. Am. Chem. Soc.* **2019**, *141*, 8473−8481.

(31) Zhou, X.; Liu, H.; Djutanta, F.; Satyabola, D.; Jiang, S. X.; Qi, X. D.; Yu, L.; Lin, S.; Hariadi, R. F.; Liu, Y.; Woodbury, N. W.; Yan, H.

https://doi.org/10.1021/jacsau.3c00826
JACS Au 2024, 4, 1125−1133

DNA-Templated Programmable Excitonic Wires for Micron-Scale Exciton Transport. *Chem.* **2022**, *8*, 2442−2459.
(32) Sovenyhazy, K. M.; Bordelon, J. A.; Petty, J. T. Spectroscopic Studies of the Multiple Binding Modes of a Trimethine-Bridged Cyanine Dye with DNA. *Nucleic Acids Res.* **2003**, *31*, 2561−2569.
(33) Karlsson, H. J.; Eriksson, M.; Perzon, E.; Akerman, B.; Lincoln, P.; Westman, G. Groove-Binding Unsymmetrical Cyanine Dyes for Staining of DNA: Syntheses and Characterization of the DNA-Binding. *Nucleic Acids Res.* **2003**, *31*, 6227−6234.
(34) Zhou, X.; Lin, S.; Yan, H. Interfacing DNA Nanotechnology and Biomimetic photonic Complexes: Advances and Prospects in Energy and Biomedicine. *J. Nanobiotechnol.* **2022**, *20*, 257.
(35) Chen, B.; Huang, Q. L.; Qu, Z. B.; Li, C.; Li, Q.; Shi, J. Y.; Fan, C. H.; Wang, L. H.; Zuo, X. L.; Shen, J. L.; Li, J. Probing Transient DNA Conformation Changes with an Intercalative Fluorescent Excimer. *Angew. Chem., Int. Ed.* **2021**, *60*, 6624−6630.
(36) Kaur, A.; Lim, Z.; Yang, K.; New, E. J. 8.14 - Fluorescent Sensors for Biological Metal Ions. In *Comprehensive Supramolecular Chemistry II*, Atwood, J. L., Ed.; Elsevier, 2017; 295−317 DOI: 10.1016/B978-0-12-409547-2.12612-5.
(37) Ke, Y. G.; Ong, L. L.; Sun, W.; Song, J.; Dong, M. D.; Shih, W. M.; Yin, P. DNA Brick Crystals with Prescribed Depths. *Nat. Chem.* **2014**, *6*, 994−1002.
(38) Wang, M.; Silva, G. L.; Armitage, B. A. DNA-Templated Formation of a Helical Cyanine Dye J-Aggregate. *J. Am. Chem. Soc.* **2000**, *122*, 9977−9986.
(39) Yuan, Y.; Li, H.; Yang, H.; Han, C.; Hu, H.; Govorov, A. O.; Yan, H.; Lan, X. Unraveling the Complex Chirality Evolution in DNA-Assembled High-Order, Hybrid Chiroplasmonic Superstructures from Multi-Scale Chirality Mechanisms. *Angew. Chem., Int. Ed.* **2022**, *61*, e202210730.
(40) Garbett, N. C.; Ragazzon, P. A.; Chaires, J. B. Circular dichroism to Determine Binding Mode and Affinity of Ligand-DNA Interactions. *Nat. Protoc.* **2007**, *2*, 3166−3172.
(41) Moon, J.-H.; Kim, S. K.; Sehlstedt, U.; Rodger, A.; Nordén, B. DNA Structural Features Responsible for Sequence-Dependent Binding Geometries of Hoechst 33258. *Biopolymers* **1996**, *38*, 593−606.
(42) Kapuściński, J.; Skoczylas, B. Fluorescent Complexes of DNA with DAPI 4′,6-Diamidine-2-Phenyl Indole 2HCl or DCI 4′,6-Dicarboxyamide-2-Pnenyl Indole. *Nucleic Acids Res.* **1978**, *5*, 3775−3800.
(43) Chiriboga, M.; Diaz, S. A.; Mathur, D.; Hastman, D. A.; Melinger, J. S.; Veneziano, R.; Medintz, I. L. Understanding Self-Assembled Pseudoisocyanine Dye Aggregates in DNA nanostructures and Their Exciton Relay Transfer Capabilities. *J. Phys. Chem. B* **2022**, *126*, 110−122.
(44) Chiriboga, M.; Green, C. M.; Mathur, D.; Hastman, D. A.; Melinger, J. S.; Veneziano, R.; Medintz, I. L.; Díaz, S. A. Structural and Optical Variation of Pseudoisocyanine Aggregates Nucleated on DNA Substrates. *Methods Appl. in Fluoresc.* **2023**, *11*, No. 014003.
(45) Würthner, F. Aggregation-Induced Emission (AIE): A Historical Perspective. *Angew. Chem., Int. Ed.* **2020**, *59*, 14192−14196.
(46) Achyuthan, K. E.; Lu, L.; Lopez, G. P.; Whitten, D. G. Supramolecular photochemical self-assemblies for fluorescence "turn on" and "turn off" assays for chem-bio-helices. *Photochem. Photobiol. Sci.* **2006**, *5*, 931−937.
(47) Hannah, K. C.; Armitage, B. A. DNA-Templated Assembly of Helical Cyanine Dye Aggregates: A Supramolecular Chain Polymerization. *Acc. Chem. Res.* **2004**, *37*, 845−853.
(48) Sen, D.; Gilbert, W. Formation of Parallel Four-Stranded Complexes by Guanine-Rich Motifs in DNA and Its Implications for Meiosis. *Nature* **1988**, *334*, 364−366.
(49) Simonsson, T. G-Quadruplex DNA Structures Variations on a Theme. *Biol. Chem.* **2001**, *382*, 621−628.
(50) Rhodes, D.; Lipps, H. J. G-Quadruplexes and Their Regulatory Roles in Biology. *Nucleic Acids Res.* **2015**, *43*, 8627−8637.
(51) Varshney, D.; Spiegel, J.; Zyner, K.; Tannahill, D.; Balasubramanian, S. The Regulation and Functions of DNA and RNA G-Quadruplexes. *Nat. Rev. Mol. Cell Biol.* **2020**, *21*, 459−474.
(52) Chung, W. J.; Heddi, B.; Schmitt, E.; Lim, K. W.; Mechulam, Y.; Phan, A. T. Structure of a Left-Handed DNA G-Quadruplex. *Proc. Natl. Acad. Sci. U.S.A.* **2015**, *112*, 2729−2733.
(53) Pandith, A.; Luo, Y.; Jang, Y.; Bae, J.; Kim, Y. Self-Assembled Peptidyl Aggregates for the Fluorogenic Recognition of Mitochondrial DNA G-Quadruplexes. *Angew. Chem., Int. Ed.* **2022**, *62*, e202215049.
(54) Chen, J. Y.; Hickey, B. L.; Wang, L. L.; Lee, J. W.; Gill, A. D.; Favero, A.; Pinalli, R.; Dalcanale, E.; Hooley, R. J.; Zhong, W. W. Selective Discrimination and Classification of G-Quadruplex Structures with a Host-Guest Sensing Array. *Nat. Chem.* **2021**, *13*, 488−495.
(55) Marchand, A.; Gabelica, V. Folding and Misfolding Pathways of G-Quadruplex DNA. *Nucleic Acids Res.* **2016**, *44*, 10999−11012.

https://doi.org/10.1021/jacsau.3c00826
JACS Au 2024, 4, 1125−1133